

Bottom-Up Synthesis of Heteroatom-Doped Chiral Graphene Nanoribbons

Xiao-Ye Wang, José I. Urgel, Gabriela Borin Barin, Kristjan Eimre, Marco Di
Giovannantonio, Alberto Milani, Matteo Tommasini, Carlo A. Pignedoli, Pascal
Ruffieux, Xinliang Feng, Roman Fasel, Klaus Müllen, and Akimitsu Narita

J. Am. Chem. Soc., **Just Accepted Manuscript** • DOI: 10.1021/jacs.8b06210 • Publication Date (Web): 10 Jul 2018

Downloaded from <http://pubs.acs.org> on July 11, 2018

Just Accepted

“Just Accepted” manuscripts have been peer-reviewed and accepted for publication. They are posted online prior to technical editing, formatting for publication and author proofing. The American Chemical Society provides “Just Accepted” as a service to the research community to expedite the dissemination of scientific material as soon as possible after acceptance. “Just Accepted” manuscripts appear in full in PDF format accompanied by an HTML abstract. “Just Accepted” manuscripts have been fully peer reviewed, but should not be considered the official version of record. They are citable by the Digital Object Identifier (DOI®). “Just Accepted” is an optional service offered to authors. Therefore, the “Just Accepted” Web site may not include all articles that will be published in the journal. After a manuscript is technically edited and formatted, it will be removed from the “Just Accepted” Web site and published as an ASAP article. Note that technical editing may introduce minor changes to the manuscript text and/or graphics which could affect content, and all legal disclaimers and ethical guidelines that apply to the journal pertain. ACS cannot be held responsible for errors or consequences arising from the use of information contained in these “Just Accepted” manuscripts.

Bottom-Up Synthesis of Heteroatom-Doped Chiral Graphene Nanoribbons

Xiao-Ye Wang,^{†§} José I. Urgel,^{‡§} Gabriela Borin Barin,[‡] Kristijan Eimre,[‡] Marco Di Giovannantonio,[‡] Alberto Milani,[⊥] Matteo Tommasini,[#] Carlo A. Pignedoli,[‡] Pascal Ruffieux,[‡] Xinliang Feng,^{||} Roman Fasel,^{*,‡,∇} Klaus Müllen,^{*,†} Akimitsu Narita^{*,†}

[†] Max Planck Institute for Polymer Research, Ackermannweg 10, 55128 Mainz, Germany

[‡] Empa, Swiss Federal Laboratories for Materials Science and Technology, 8600 Dübendorf, Switzerland

[⊥] Dipartimento di Energia, Politecnico di Milano, Via Ponzio 34-3, 20133 Milano, Italy

[#] Dipartimento di Chimica, Materiali e Ingegneria Chimica ‘G. Natta’, Politecnico di Milano, Piazza Leonardo da Vinci 32, 20133 Milano, Italy

^{||} Center for Advancing Electronics Dresden, Department of Chemistry and Food Chemistry, Technische Universität Dresden, 01062 Dresden, Germany

[∇] Department of Chemistry and Biochemistry, University of Bern, 3012 Bern, Switzerland

Supporting Information Placeholder

ABSTRACT: Bottom-up synthesis of graphene nanoribbons (GNRs) has significantly advanced during the past decade, providing various GNR structures with tunable properties. The synthesis of chiral GNRs, however, has been underexplored, and only limited to (3,1)-GNRs. We report herein the surface-assisted synthesis of the first heteroatom-doped chiral (4,1)-GNRs from the rationally designed precursor 6,16-dibromo-9,10,19,20-tetraoxa-9a,19a-diboratetraperylene. The structure of the chiral GNRs has been verified by scanning tunneling microscopy, non-contact atomic force microscopy, and Raman spectroscopy in combination with theoretical modeling. Due to the presence of oxygen-boron-oxygen (OBO) segments on the edges, lateral self-assembly of the GNRs has been observed, realizing well-aligned GNR arrays with different modes of homochiral and heterochiral inter-ribbon assemblies.

Due to their width-dependent bandgap, graphene nanoribbons (GNRs), nanometer-wide strips of graphene, have been recognized as a promising material for next-generation semiconductor device applications.¹ Bottom-up synthesis of GNRs has proven a powerful tool to fabricate atomically precise graphene nanostructures by synthetic design.² In particular, the on-surface synthesis under ultrahigh vacuum (UHV) conditions allows for the fabrication of atomically precise GNRs with different edge structure and width.³ In recent years, armchair GNRs (AGNRs)⁴ have been extensively investigated, confirming the expected width-dependent bandgaps, and the long-pursued zigzag GNRs (ZGNRs)⁵ possessing localized edge states have also been achieved (Figure 1a,b). On the other hand, chiral GNRs (CGNRs) with a combination of armchair and zigzag edges have been largely underexplored, although they represent an important class of the GNR family (Figure 1c).⁶ The edge configuration of CGNRs is described by a translation vector (n,m) of the graphene lattice, and different chiral indices (n,m) result in distinct

electronic properties.⁷ So far, however, only the synthesis of (3,1)-GNRs has been achieved from 9,9'-bianthracene-based molecular precursors, and the investigations of bottom-up synthesized CGNRs have been limited to this particular structure.⁸ Further precise variations of the chiral edges have remained elusive.

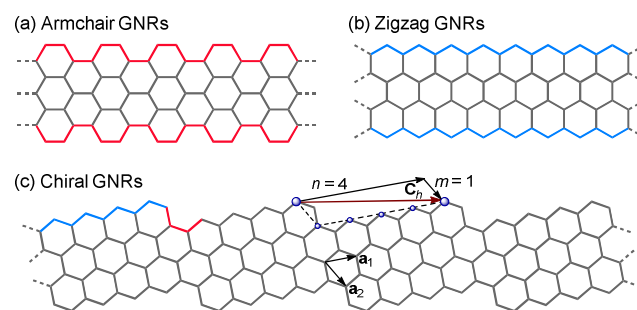


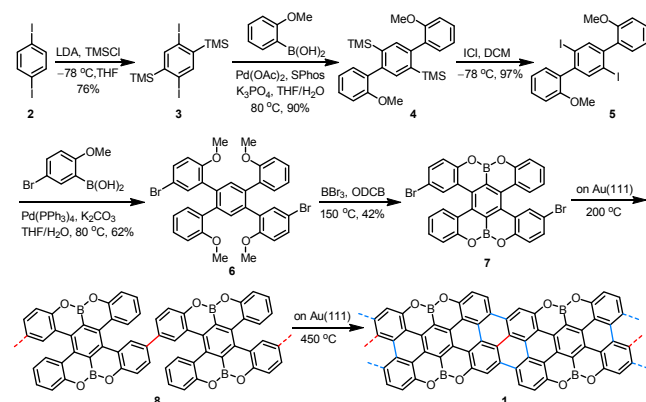
Figure 1. Representation of the three classes of graphene nanoribbons (GNRs). (a) Armchair GNRs (AGNRs). (b) Zigzag GNRs (ZGNRs). (c) Chiral GNRs (CGNRs). The edge geometry of CGNRs is characterized by the translation vector C_h , defined as $C_h = n\mathbf{a}_1 + m\mathbf{a}_2 = (n,m)$, where \mathbf{a}_1 and \mathbf{a}_2 are the unit vectors of the graphene lattice. An exemplary case of the chiral (4,1)-GNR is illustrated.

Furthermore, incorporating heteroatom dopants into GNRs via the bottom-up approach can finely modulate their band structure and electronic properties, as well as their self-assembly behavior.⁹ Major achievements on heteroatom-doped GNRs include chevron-type GNRs with nitrogen,⁹⁻¹⁰ sulfur,^{10d,11} or oxygen^{10d} atoms on the edges, and AGNRs with boron dopants¹² or boron-nitrogen co-dopants¹³ inside the backbone as well as sulfur¹⁴ or nitrogen¹⁵ atoms on the edges. Nevertheless, heteroatom doping in other types of GNRs, e.g. ZGNRs and CGNRs, has not hitherto been explored. Herein, we report the bottom-up synthesis and characterization of the first heteroatom-doped (4,1)-GNRs using

the rationally designed molecular precursor 6,16-dibromo-9,10,19,20-tetraoxa-9a,19a-diboratetrazabenz[*a,f,j,o*]perylene (compound **7** in Scheme 1). The monomer features stable zigzag edges substituted with OBO units,¹⁶ and the resulting GNRs represent the first case of OBO-doped GNRs.

The synthetic route to OBO-doped chiral (4,1)-GNR **1** is described in Scheme 1. 1,4-Diiodobenzene (**2**) was first deprotonated by lithium diisopropylamide (LDA) and then reacted with trimethylsilyl chloride (TMSCl) to provide 1,4-diiodo-2,5-bis(trimethylsilyl)benzene (**3**) in 76% yield. Suzuki coupling of **3** with (2-methoxyphenyl)boronic acid afforded 1,4-bis(trimethylsilyl)-2,5-bis(2'-methoxyphenyl)benzene (**4**) in 90% yield. Subsequently, the TMS groups on **4** were efficiently transformed into iodo groups by treatment with iodine monochloride (ICl) to give 1,4-diiodo-2,5-bis(2'-methoxyphenyl)benzene (**5**), which was subjected to another Suzuki coupling with (5-bromo-2-methoxyphenyl)boronic acid to produce 1,4-bis(5'-bromo-2'-methoxyphenyl)-2,5-bis(2'-methoxyphenyl)benzene (**6**) in 62% yield. Then a tandem demethylation-borylation reaction¹⁶ was applied to **6** with BBr₃ in *o*-dichlorobenzene (ODCB) to give monomer **7** in 42% yield. Monomer **7** was characterized by ¹H and ¹³C NMR spectroscopies and high-resolution mass spectrometry.

Scheme 1. Synthetic Route to the Chiral (4,1)-GNR **1**.



To fabricate the OBO-doped chiral (4,1)-GNR **1**, monomer **7** was first sublimed onto an Au(111) substrate held at room temperature under UHV conditions. Constant-current scanning tunneling microscopy (STM) images of the resulting molecular layer reveal intact monomers self-assembled into linear chains (see Figure S1 in the Supporting Information). A closer look allows one to discern R and S enantiomers within the same chain, stabilized mainly by lateral intermolecular O \cdots H interactions¹⁷ with a projected length of 3.5 ± 0.3 Å. Additionally, Br \cdots H interactions with a projected length of 2.7 ± 0.2 Å, forming assembled structures along the perpendicular dimension, were also observed (see Figure S1, where lateral intermolecular lengths were obtained from properly scaled atomistic models of the STM images). Annealing of the substrate at 200 °C induced aryl-aryl coupling, forming 1D polymer **8** after dehalogenation of **7**. Importantly, single chirality of monomers, assembled side by side, was preserved within each polymeric chain (Figure 2a). This fact is attributed to steric repulsion between monomers with opposite chirality inhibiting the aryl-aryl coupling between them. A closer view of a single polymeric chain reveals a periodic appearance of bright protrusions (apparent height of 2.4 Å), which result from the highly nonplanar geometry adopted by the polymer due to the steric hindrance between the H atoms in neighboring units (Figure 2b).^{8c} The periodic distance of these bright protrusions in the STM image is 11.2 Å, in good agreement with the structural

model (11.0 Å, Figure 2c), demonstrating the successful polymerization.

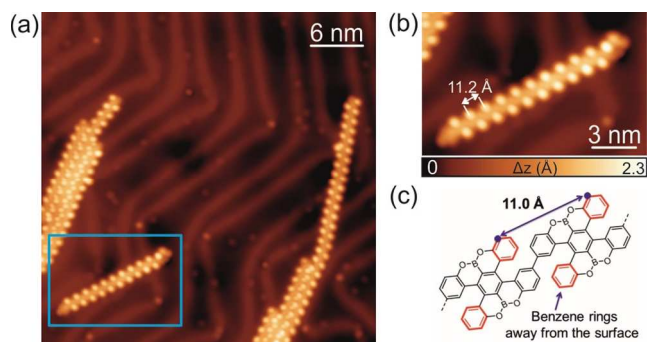


Figure 2. STM images of monomer **7** after annealing at 200 °C on Au(111), inducing debromination and polymerization. (a) Large-scale STM image of the resulting polymer **8**. (b) Magnified view of the single polymeric chain shown in panel a evidencing the presence of periodic bright protrusions. Scanning conditions: $V_b = -1.5$ V, $I = 20$ pA. (c) Structural model of polymer **8**. The benzene rings in red correspond to the bright protrusions in panels a and b.

Further annealing of the substrate at 400 °C induced minor modifications of the 1D polymeric chains, which are attributed to the onset of the cyclodehydrogenation reaction (see Figure S2). Finally, annealing the sample at 450 °C completed cyclodehydrogenation, providing the fully planarized OBO-doped (4,1)-GNR **1** with an apparent height of 1.8 Å (Figure 3a,b) and an average length of 61 nm (see the histogram in Figure S3). To confirm the chemical structure of the resulting CGNRs, non-contact atomic force microscopy (nc-AFM) measurements using a CO-functionalized tip were performed.¹⁸ Figure 3c depicts the resulting constant-height frequency-shift image where the periodic aromatic carbon atoms together with the oxygen atoms are clearly unveiled, while the boron atoms appear with a darker contrast (more negative frequency shift) due to a stronger interaction with the gold substrate as previously reported by Kawai *et al.* in the formation of boron-doped AGNRs.^{12a} It is worthwhile mentioning that the OBO-doped CGNRs are found to laterally align on the Au(111) substrate. The regular alignment of GNRs arises from inter-ribbon O \cdots H interactions¹⁷ (see Figure S4 for STM images and corresponding atomistic models of homochiral and heterochiral inter-ribbon interactions) and illustrates a particular aspect of heteroatom-doped GNRs, which can be of crucial importance for future device applications. To gain more insight into the lateral alignment of OBO-doped (4,1)-GNR **1**, density functional theory (DFT) calculations were performed on the self-assembled structures (Figure 3d,e). The interaction energy of two OBO-doped CGNRs of opposite chirality is -0.30 eV/unit cell with O \cdots H interaction distances of 2.43 and 2.72 Å, in good agreement with experimental data. In the case of two OBO-doped CGNRs with the same chirality, the interaction energy is -0.24 eV/unit cell with O \cdots H interaction distances of 2.28 and 3.49 Å. These computational results suggest that the interaction of ribbons with opposite chirality is stronger than that of ribbons with the same chirality, though no clear experimental preference in the interaction of ribbons with the same/different chirality has been found. In addition, we have computed the interaction energy of the structurally equivalent pristine (4,1)-GNR to be -0.10 eV/unit cell, indicating that the OBO units on the edges endow the GNRs with stronger inter-ribbon interactions.

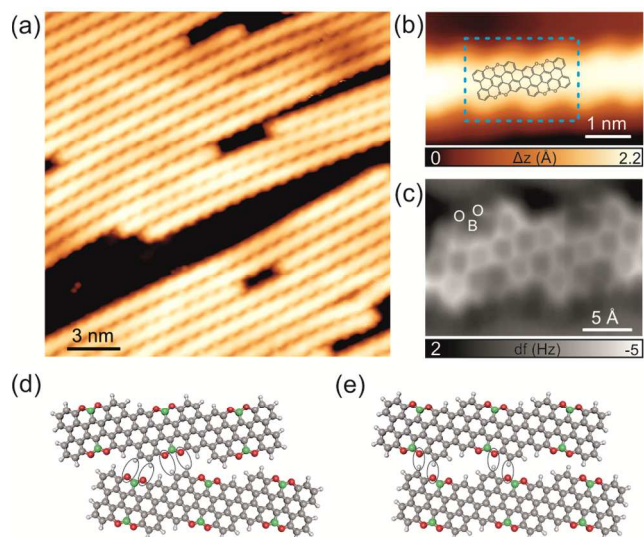


Figure 3. Formation of OBO-doped (4,1)-GNR **1** on Au(111) after annealing at 450 °C. (a) STM overview of (4,1)-GNR **1**. $V_b = 0.1$ V, $I = 70$ pA. (b) High-resolution STM image of a single ribbon with the chemical structure of a segment superimposed. $V_b = -1.5$ V, $I = 50$ pA. (c) Constant-height frequency-shift nc-AFM image of the ribbon segment reported in the dashed blue rectangle of panel b acquired with a CO-functionalized tip (z offset -20 pm below STM set point: -5 mV, 10 pA). (d,e) DFT models of inter-ribbon interactions for heterochiral and homochiral (4,1)-GNRs, respectively.

Next, scanning tunneling spectroscopy (STS) studies were performed on (4,1)-GNR **1** and its differential conductance (dI/dV) spectra were recorded. The conduction band minimum and the valence band minimum are clearly identified at 1.77 eV and -1.56 eV, respectively, corresponding to a STS-bandgap of 3.33 eV (Figure S5). This is in good agreement with the bandgap of 2.96 eV, calculated within the image charge corrected¹⁹ GW approximation.²⁰ Additionally, DFT calculations reveal that the OBO-doped (4,1)-GNR **1** exhibits a larger bandgap (1.50 eV) in vacuum compared with the pristine all-carbon (4,1)-GNR (0.50 eV). This can be explained by the weak conjugation of the p_z orbitals of the OBO segments with the extended π -system of the carbon backbone of the GNR. Although weak, this conjugation lowers the bandgap with respect to that of the GNR without OBO units by 0.40 eV (1.90 eV) (see Figure S6 for details).

Finally, we used Raman spectroscopy to further characterize the fabricated (4,1)-GNRs. Raman spectra were measured in ambient conditions with an excitation wavelength of 532 nm (2.33 eV) on Au (111). To assign the observed Raman lines, DFT calculations were performed (Figure 4). The DFT-simulated spectrum agrees well with the experimental data, further confirming the structure of (4,1)-GNR **1** and indicating that the GNR structure is preserved in ambient conditions. Interestingly, DFT calculations reveal that the typical D-mode vibrations localize on two different regions of the (4,1)-GNR, namely the armchair (A) and zigzag (Z) segments of the ribbon. Therefore, the D signal splits into two components arising from the A and Z regions (1325 cm^{-1} and 1481 cm^{-1} , respectively). Similarly, the G band exhibits contributions from the A and Z segments, which both display longitudinal ($G_{A,l}$ and $G_{Z,l}$) and transversal ($G_{A,t}$ and $G_{Z,t}$) components (Figure 4, see Figure S7 and S8 for details).

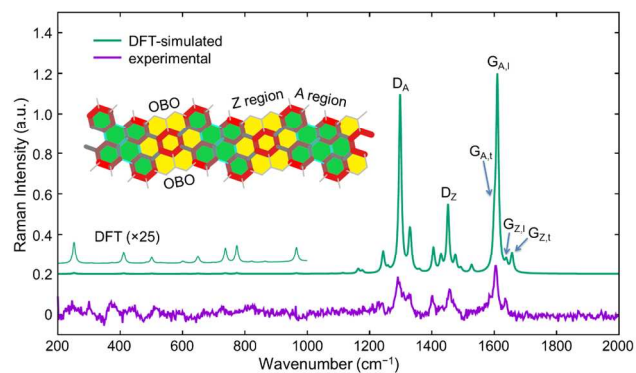


Figure 4. Experimental and DFT-simulated Raman spectra of (4,1)-GNR **1**. The model of a GNR segment is shown in the inset, with the zigzag (Z) region marked in yellow and the armchair (A) region in green. The wavenumber axis of the simulated Raman spectrum has been uniformly scaled by a factor of 0.98 to ease comparison with the experimental data.

In summary, we have synthesized the first chiral (4,1)-GNR with OBO heteroatoms on the edges via the bottom-up on-surface synthesis. The GNR structure has been unambiguously characterized by STM and nc-AFM, as well as Raman spectroscopy. STS studies together with theoretical calculations revealed that the OBO-doped (4,1)-GNRs exhibit a larger bandgap than the pristine (4,1)-GNRs, but a lowered bandgap relative to the GNRs without OBO segments. The synthetic strategy demonstrated in this work paves the way to further variation of the chiral indices of GNRs, which is essential for the development of GNR-based materials. Furthermore, this work represents the first case of OBO-doped GNRs, indicating that the OBO segments on the edges endow the GNRs with unique self-assembly properties, achieving lateral alignment of GNRs. Such alignment may be of importance for future GNR-based devices to increase the bridging probability between the electrodes and enhance charge transport efficiency.

ASSOCIATED CONTENT

Supporting Information

The Supporting Information is available free of charge on the ACS Publications website.

Procedures of solution synthesis, experimental details and data, theoretical simulations (PDF)

AUTHOR INFORMATION

Corresponding Author

*muellen@mpip-mainz.mpg.de

*roman.fasel@empa.ch

*narita@mpip-mainz.mpg.de

Author Contributions

[§]These authors contributed equally.

Notes

The authors declare no competing financial interests.

ACKNOWLEDGMENT

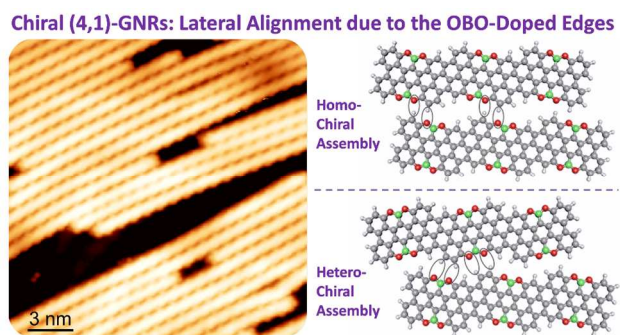
We thank the financial support from the Max Planck Society, the European Union's Horizon 2020 research and innovation programme under GrapheneCore1 (No 696656) and GrapheneCore2 (No 785219), and NCCR MARVEL funded by the Swiss National Science Foundation. The Swiss

Supercomputing Center (CSCS project s746) and PRACE project 2016153518 are acknowledged for computational resources. A.M. and M.T. acknowledge funding support from the European Research Council (ERC) under the European Union's Horizon 2020 research and innovation programme ERC–Consolidator Grant (ERC CoG 2016 EspLORE grant agreement No 724610).

REFERENCES

- (1) (a) Wang, X.-Y.; Narita, A.; Müllen, K. *Nat. Rev. Chem.* **2017**, *2*, 0100; (b) Schwierz, F. *Nat. Nanotech.* **2010**, *5*, 487; (c) Castro Neto, A. H.; Guinea, F.; Peres, N. M. R.; Novoselov, K. S.; Geim, A. K. *Rev. Mod. Phys.* **2009**, *81*, 109; (d) Obradovic, B.; Kotlyar, R.; Heinz, F.; Matagne, P.; Rakshit, T.; Giles, M. D.; Stettler, M. A.; Nikonov, D. E. *Appl. Phys. Lett.* **2006**, *88*, 142102.
- (2) Narita, A.; Wang, X.-Y.; Feng, X.; Müllen, K. *Chem. Soc. Rev.* **2015**, *44*, 6616.
- (3) Talirz, L.; Ruffieux, P.; Fasel, R. *Adv. Mater.* **2016**, *28*, 6222.
- (4) (a) Yang, X.; Dou, X.; Rouhanipour, A.; Zhi, L.; Räder, H. J.; Müllen, K. *J. Am. Chem. Soc.* **2008**, *130*, 4216; (b) Cai, J.; Ruffieux, P.; Jaafar, R.; Bieri, M.; Braun, T.; Blankenburg, S.; Muoth, M.; Seitsonen, A. P.; Saleh, M.; Feng, X.; Müllen, K.; Fasel, R. *Nature* **2010**, *466*, 470; (c) Chen, Y.-C.; de Oteyza, D. G.; Pedramrazi, Z.; Chen, C.; Fischer, F. R.; Crommie, M. F. *ACS Nano* **2013**, *7*, 6123; (d) Basagni, A.; Sedona, F.; Pignedoli, C. A.; Cattelan, M.; Nicolas, L.; Casarin, M.; Sambri, M. *J. Am. Chem. Soc.* **2015**, *137*, 1802; (e) Zhang, H.; Lin, H.; Sun, K.; Chen, L.; Zagariyarski, Y.; Aghdassi, N.; Duhm, S.; Li, Q.; Zhong, D.; Li, Y.; Müllen, K.; Fuchs, H.; Chi, L. *J. Am. Chem. Soc.* **2015**, *137*, 4022; (f) Gao, J.; Uribe-Romo, F. J.; Saathoff, J. D.; Arslan, H.; Crick, C. R.; Hein, S. J.; Itin, B.; Clancy, P.; Dichtel, W. R.; Loo, Y.-L. *ACS Nano* **2016**, *10*, 4847; (g) Jordan, R. S.; Wang, Y.; McCurdy, R. D.; Yeung, M. T.; Marsh, K. L.; Khan, S. I.; Kaner, R. B.; Rubin, Y. *Chem* **2016**, *1*, 78; (h) Li, G.; Yoon, K.-Y.; Zhong, X.; Zhu, X.; Dong, G. *Chem. Eur. J.* **2016**, *22*, 9116; (i) Yang, W.; Lucotti, A.; Tommasini, M.; Chalifoux, W. A. *J. Am. Chem. Soc.* **2016**, *138*, 9137; (j) Jordan, R. S.; Li, Y. L.; Lin, C.-W.; McCurdy, R. D.; Lin, J. B.; Brosmer, J. L.; Marsh, K. L.; Khan, S. I.; Houk, K. N.; Kaner, R. B.; Rubin, Y. *J. Am. Chem. Soc.* **2017**, *139*, 15878; (k) Talirz, L.; Söde, H.; Dumschlaff, T.; Wang, S.; Sanchez-Valencia, J. R.; Liu, J.; Shinde, P.; Pignedoli, C. A.; Liang, L.; Meunier, V.; Plumb, N. C.; Shi, M.; Feng, X.; Narita, A.; Müllen, K.; Fasel, R.; Ruffieux, P. *ACS Nano* **2017**, *11*, 1380.
- (5) Ruffieux, P.; Wang, S.; Yang, B.; Sánchez-Sánchez, C.; Liu, J.; Dienel, T.; Talirz, L.; Shinde, P.; Pignedoli, C. A.; Passerone, D.; Dumschlaff, T.; Feng, X.; Müllen, K.; Fasel, R. *Nature* **2016**, *531*, 489.
- (6) (a) Tao, C.; Jiao, L.; Yazyev, O. V.; Chen, Y.-C.; Feng, J.; Zhang, X.; Capaz, R. B.; Tour, J. M.; Zettl, A.; Louie, S. G.; Dai, H.; Crommie, M. F. *Nat. Phys.* **2011**, *7*, 616; (b) Yazyev, O. V.; Capaz, R. B.; Louie, S. G. *Phys. Rev. B* **2011**, *84*, 115406; (c) Golor, M.; Lang, T. C.; Wessel, S. *Phys. Rev. B* **2013**, *87*, 155441.
- (7) Carvalho, A. R.; Warnes, J. H.; Lewenkopf, C. H. *Phys. Rev. B* **2014**, *89*, 245444.
- (8) (a) Han, P.; Akagi, K.; Federici Canova, F.; Mutoh, H.; Shiraki, S.; Iwaya, K.; Weiss, P. S.; Asao, N.; Hitosugi, T. *ACS Nano* **2014**, *8*, 9181; (b) Han, P.; Akagi, K.; Federici Canova, F.; Shimizu, R.; Oguchi, H.; Shiraki, S.; Weiss, P. S.; Asao, N.; Hitosugi, T. *ACS Nano* **2015**, *9*, 12035; (c) de Oteyza, D. G.; García-Lekue, A.; Vilas-Varela, M.; Merino-Díez, N.; Carbonell-Sanromà, E.; Corso, M.; Vasseur, G.; Rogero, C.; Guitián, E.; Pascual, J. I.; Ortega, J. E.; Wakayama, Y.; Peña, D. *ACS Nano* **2016**, *10*, 9000; (d) Sánchez-Sánchez, C.; Dienel, T.; Deniz, O.; Ruffieux, P.; Berger, R.; Feng, X.; Müllen, K.; Fasel, R. *ACS Nano* **2016**, *10*, 8006; (e) Merino-Díez, N.; Li, J.; García-Lekue, A.; Vasseur, G.; Vilas-Varela, M.; Carbonell-Sanromà, E.; Corso, M.; Ortega, J. E.; Peña, D.; Pascual, J. I.; de Oteyza, D. G. *J. Phys. Chem. Lett.* **2018**, *9*, 25; (f) Schulz, F.; Jacobse, P. H.; Canova, F. F.; van der Lit, J.; Gao, D. Z.; van den Hoogenband, A.; Han, P.; Klein Gebbink, R. J. M.; Moret, M.-E.; Joensuu, P. M.; Swart, I.; Liljeroth, P. *J. Phys. Chem. C* **2017**, *121*, 2896.
- (9) Cai, J.; Pignedoli, C. A.; Talirz, L.; Ruffieux, P.; Söde, H.; Liang, L.; Meunier, V.; Berger, R.; Li, R.; Feng, X.; Müllen, K.; Fasel, R. *Nat. Nanotech.* **2014**, *9*, 896.
- (10) (a) Bronner, C.; Strelau, S.; Gille, M.; Brauße, F.; Haase, A.; Hecht, S.; Tegeder, P. *Angew. Chem. Int. Ed.* **2013**, *52*, 4422; (b) Zhang, Y.; Zhang, Y.; Li, G.; Lu, J.; Lin, X.; Du, S.; Berger, R.; Feng, X.; Müllen, K.; Gao, H.-J. *Appl. Phys. Lett.* **2014**, *105*, 023101; (c) Vo, T. H.; Shekhirev, M.; Kunkel, D. A.; Orange, F.; Guinel, M. J. F.; Enders, A.; Sinitiskii, A. *Chem. Commun.* **2014**, *50*, 4172; (d) Durr, R. A.; Haberer, D.; Lee, Y.-L.; Blackwell, R.; Kalayjian, A. M.; Marangoni, T.; Ihm, J.; Louie, S. G.; Fischer, F. R. *J. Am. Chem. Soc.* **2018**, *140*, 807–813; (e) Marangoni, T.; Haberer, D.; Rizzo, D. J.; Cloke, R. R.; Fischer, F. R. *Chem. Eur. J.* **2016**, *22*, 13037; (f) Vo, T. H.; Perera, U. G. E.; Shekhirev, M.; Mehdi Pour, M.; Kunkel, D. A.; Lu, H.; Gruverman, A.; Sutter, E.; Cotlet, M.; Nykypanchuk, D.; Zahl, P.; Enders, A.; Sinitiskii, A.; Sutter, P. *Nano Lett.* **2015**, *15*, 5770.
- (11) Zhang, Y.-F.; Zhang, Y.; Li, G.; Lu, J.; Que, Y.; Chen, H.; Berger, R.; Feng, X.; Müllen, K.; Lin, X.; Zhang, Y.-Y.; Du, S.; Pantelides, S. T.; Gao, H.-J. *Nano Res.* **2017**, *10*, 3377.
- (12) (a) Kawai, S.; Saito, S.; Osumi, S.; Yamaguchi, S.; Foster, A. S.; Spijker, P.; Meyer, E. *Nat. Commun.* **2015**, *6*, 8098; (b) Cloke, R. R.; Marangoni, T.; Nguyen, G. D.; Joshi, T.; Rizzo, D. J.; Bronner, C.; Cao, T.; Louie, S. G.; Crommie, M. F.; Fischer, F. R. *J. Am. Chem. Soc.* **2015**, *137*, 8872.
- (13) Kawai, S.; Nakatsuka, S.; Hatakeyama, T.; Pawlak, R.; Meier, T.; Tracey, J.; Meyer, E.; Foster, A. S. *Sci. Adv.* **2018**, *4*.
- (14) (a) Nguyen, G. D.; Toma, F. M.; Cao, T.; Pedramrazi, Z.; Chen, C.; Rizzo, D. J.; Joshi, T.; Bronner, C.; Chen, Y.-C.; Favaro, M.; Louie, S. G.; Fischer, F. R.; Crommie, M. F. *J. Phys. Chem. C* **2016**, *120*, 2684; (b) Miao, D.; Daigle, M.; Lucotti, A.; Boismenu-Lavoie, J.; Tommasini, M.; Morin, J. F. *Angew. Chem. Int. Ed.* **2018**, *57*, 3588.
- (15) Carbonell-Sanromà, E.; Hieulle, J.; Vilas-Varela, M.; Brandimarte, P.; Iraola, M.; Barragán, A.; Li, J.; Abadia, M.; Corso, M.; Sánchez-Portal, D.; Peña, D.; Pascual, J. I. *ACS Nano* **2017**, *11*, 7355.
- (16) Wang, X.-Y.; Narita, A.; Zhang, W.; Feng, X.; Müllen, K. *J. Am. Chem. Soc.* **2016**, *138*, 9021.
- (17) Wang, X.-Y.; Dienel, T.; Di Giovannantonio, M.; Barin, G. B.; Kharche, N.; Deniz, O.; Urgel, J. I.; Widmer, R.; Stolz, S.; De Lima, L. H.; Muntwiler, M.; Tommasini, M.; Meunier, V.; Ruffieux, P.; Feng, X.; Fasel, R.; Müllen, K.; Narita, A. *J. Am. Chem. Soc.* **2017**, *139*, 4671.
- (18) Gross, L.; Mohn, F.; Moll, N.; Liljeroth, P.; Meyer, G. *Science* **2009**, *325*, 1110.
- (19) Neaton, J. B.; Hybertsen, M. S.; Louie, S. G. *Phys. Rev. Lett.* **2006**, *97*, 216405.
- (20) Wilhelm, J.; Golze, D.; Talirz, L.; Hutter, J.; Pignedoli, C. A. *J. Phys. Chem. Lett.* **2018**, *9*, 306.

Table of Contents Graphic



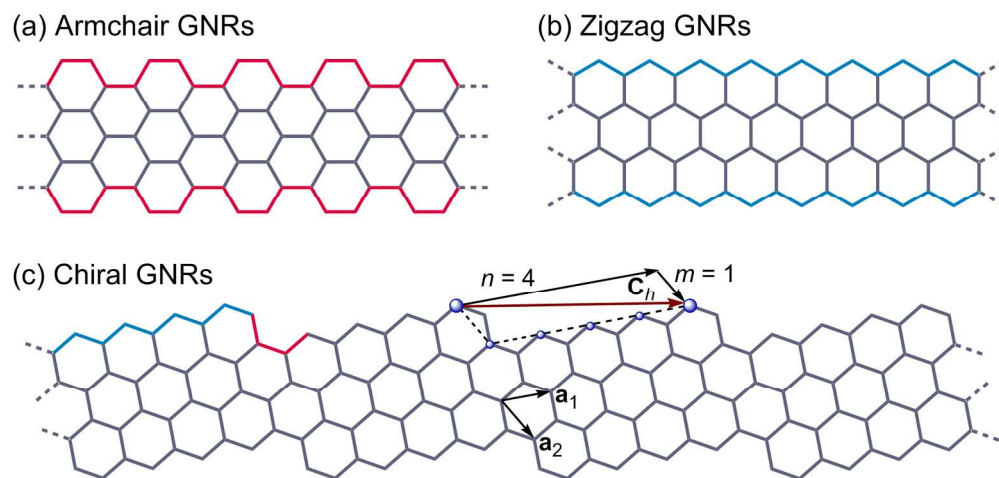


Figure 1

173x83mm (300 x 300 DPI)

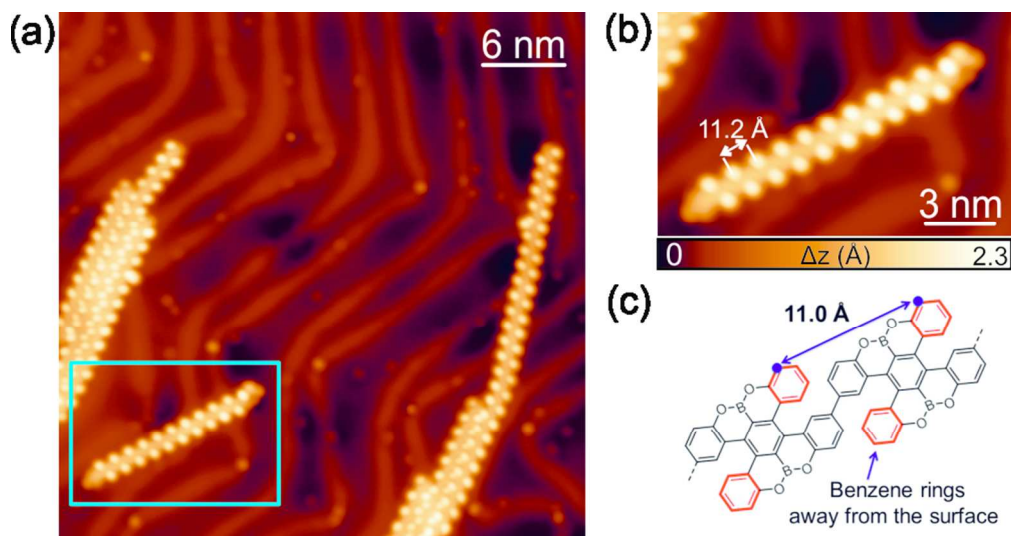


Figure 2

84x44mm (300 x 300 DPI)

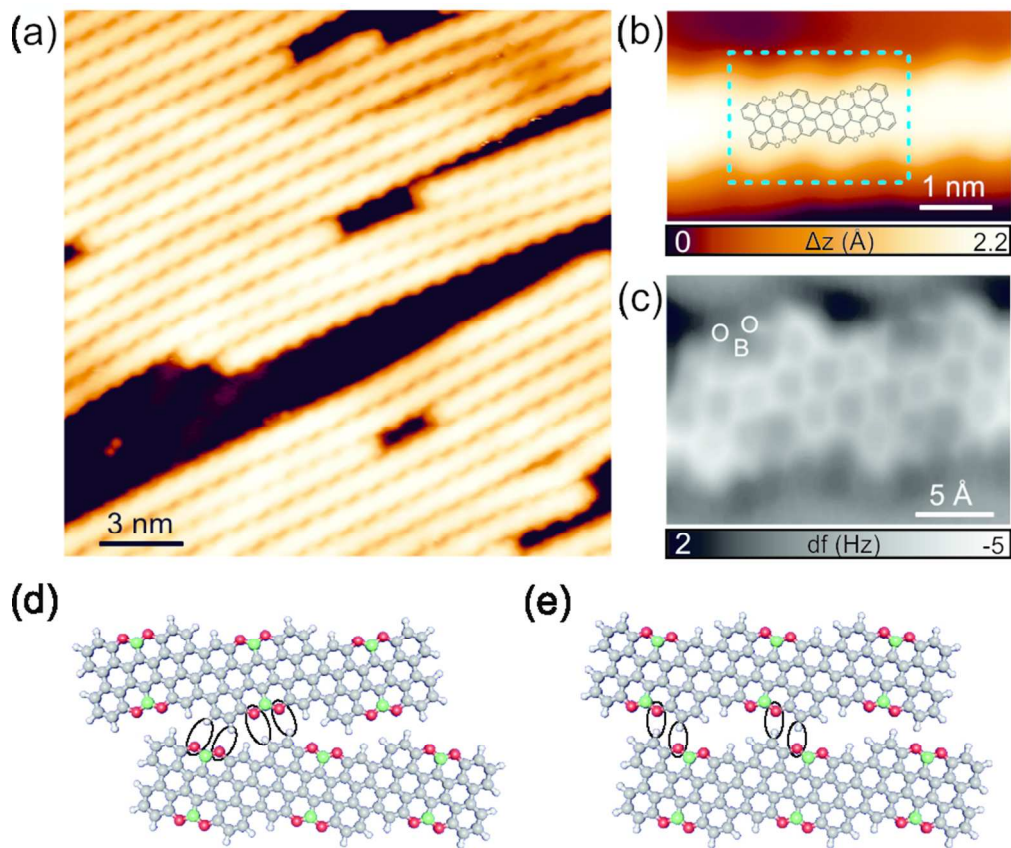


Figure 3

81x68mm (300 x 300 DPI)

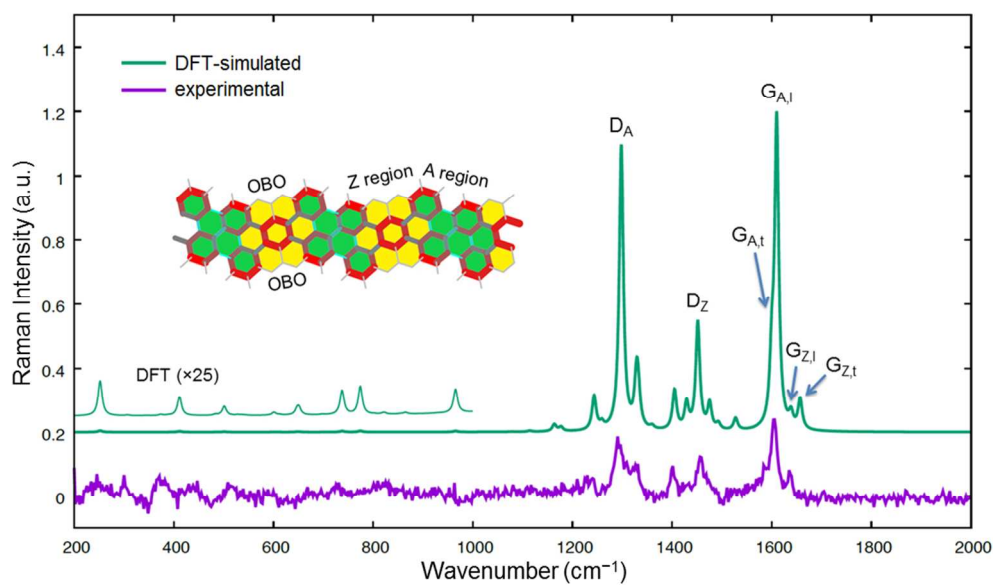
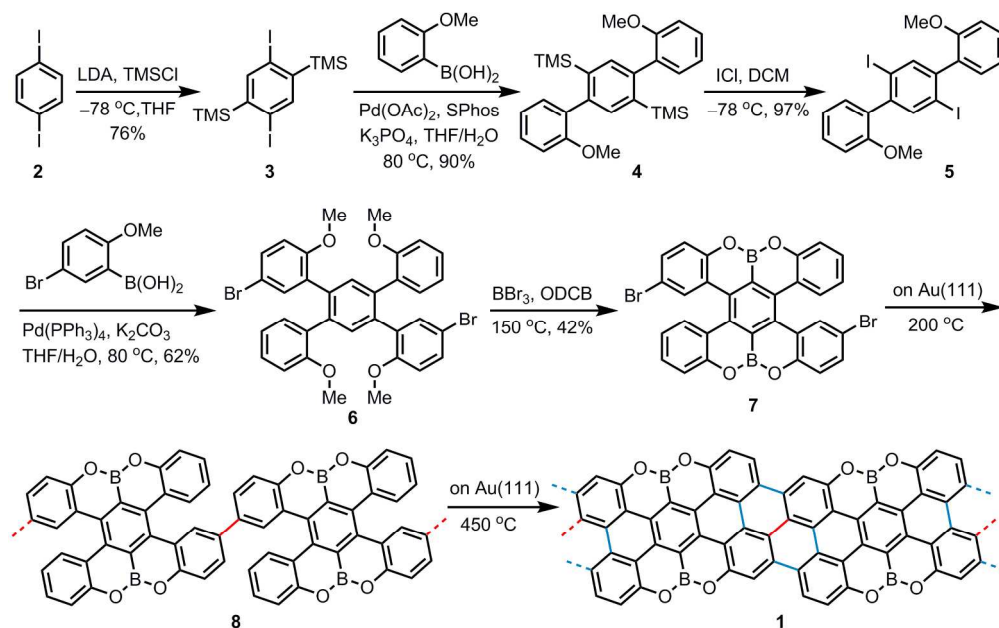


Figure 4

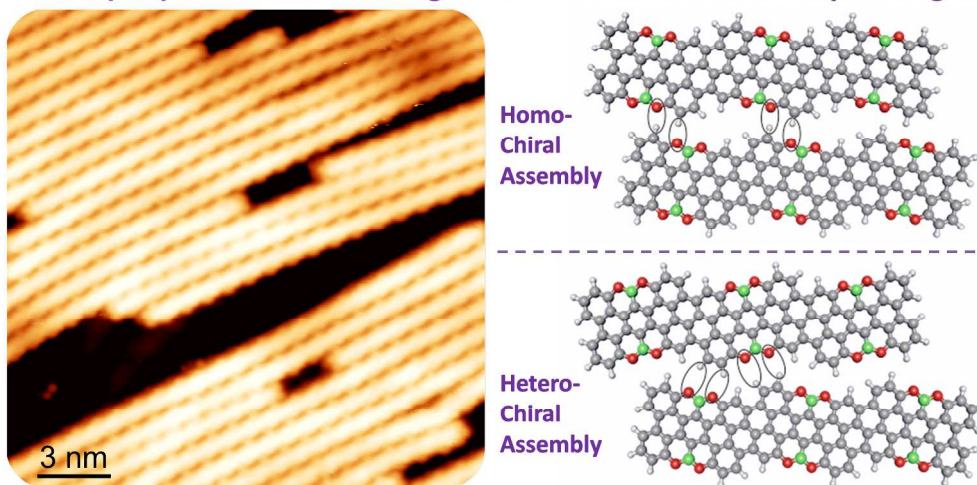
309x185mm (96 x 96 DPI)



Scheme 1

194x122mm (300 x 300 DPI)

Chiral (4,1)-GNRs: Lateral Alignment due to the OBO-Doped Edges



TOC Graphic

825x444mm (96 x 96 DPI)